Journal of Molecular Structure 1267 (2022) 133552

Contents lists available at ScienceDirect

Journal of Molecular Structure

journal homepage: www.elsevier.com/locate/molstr

# Spectroscopic (FT-IR, NMR, single crystal XRD) and DFT studies including FMO, Mulliken charges, and Hirshfeld surface analysis, molecular docking and ADME analyses of 2-amino-4′-fluorobenzophenone (FAB)

Rajendran Satheeshkumar[a,*], Kolandaivel Prabha[b], Kailasam Natesan Vennila[c], Koray Sayin[d,*], Elif Güney[d], Werner Kaminsky[e,*], Roberto Acevedo[a]

[a] Facultad de Ingeniería y Tecnología, Universidad San Sebastián, Bellavista 7, Santiago 8420524, Chile
[b] Department of Chemistry, K. S. Rangasamy College of Technology, Tiruchengode 637215, Tamil Nadu, India
[c] Department of Chemistry, The Gandhigram Rural Institute- Deemed to be University, Gandhigram 624 302, Tamil Nadu, India
[d] Department of Chemistry, Faculty of Science, Sivas Cumhuriyet University Sivas 58140, Türkiye
[e] Department of Chemistry, University of Washington, Seattle, WA 98195, USA

ARTICLE INFO

*Article history:*
Received 5 April 2022
Revised 16 June 2022
Accepted 18 June 2022
Available online 20 June 2022

*Keywords:*
2-Amino-4′-fluorobenzophenone
DFT calculations
Molecular docking studies
ADME studies

ABSTRACT

In this work, synthesis, and crystal structure of molecule 2-amino-4′-fluorobenzophenone (FAB) is confirmed by using FT-IR, FT-Raman, $^{1}H$ and $^{13}C$ NMR chemical shifts, compared with calculated parameters using B3LYP/ 6-311+G(d) basis sets in water were found in good agreement. The optimized geometry of the molecule (FAB) was compared to the experimental XRD values. DFT calculations of the molecular electrostatic potential (MEP), frontier molecular orbitals (FMO), Hirshfeld surface analysis, Mulliken charges recognize the chemically active sites of this molecule responsible for its chemical reactivity. *In silico* molecular docking analyses of molecule (FAB) have been done with vascular endothelial growth factor receptor 2 (VEGFR2) kinase inhibitors. Further, the bioavailability of molecule (FAB) was investigated by ADME and p450 analyses.



## 1. Introduction

The main pathway to discover, design, synthesize, and develop pharmaceutical drugs traditionally follows modifying a small molecule through analogue synthesis [1,2]. Numerous small molecule tyrosine kinase inhibitors of VEGF receptor 2 (VEGFR2) are approved for the treatment of various types of cancer, including renal cell carcinoma, hepatocellular carcinoma, and colorectal carcinoma [3,4]. Adaptability and significance of $\alpha$-amino ketones for ubiquitous applications is utilized through synthesis and drug discovery chemistry [5]. *o*-Aminobenzophenones have considered more attention because of their various pharmaceutical applications in medicinal chemistry [6,7], using them as a versatile intermediate for further transformations in synthetic chemistry [8,9] and their application in materials chemistry [10]. Preparation of 1,4-benzodiazepines through the key intermediate of *o*-aminobenzophenones molecules are utilized as a starting precursor by Blazevic and Kajfez [11]. *o*-Aminobenzophenones involved synthesis of quinazolines with benzylic amines in remarkable yields by utilizing copper oxide nanoparticles supported on kaolin heterogeneous catalyst [12]. In recently, the starting synthon of *o*-aminobenzophenones used for preparation of Friedländer's synthesis of quinolines in the development of bioactive heterocyclic derivatives of medicinal chemistry [13–17].

Based on the above biological aspects, we carried out the synthesis of 2-amino-4′-fluorobenzophenone (FAB) from 2-nitro-4′-fluorobenzophenone [18–20]. Quantum chemical calculations [21–31] are carried out at the B3LYP/ 6-311+G(d) levels of theory in water phase for structure optimization, vibration frequencies, highest occupied molecular orbital (HOMO) / lowest unoccupied molecular orbital (LUMO), molecular electrostatic potential (MEP) maps, Hirshfeld surface analysis, and NMR spectra. To predict biological activity of molecule (FAB), *in silico* molecular docking calculations have been used [32–36]. Here, Molecular docking is studied against PDB: 3WZE [37], which is a vascular endothelial growth

* Corresponding authors.
*E-mail addresses:* drrsatheeshphd@gmail.com (R. Satheeshkumar), krysayin@gmail.com, ksayin@cumhuriyet.edu.tr (K. Sayin), wernerka@uw.edu (W. Kaminsky).

https://doi.org/10.1016/j.molstruc.2022.133552
0022-2860/

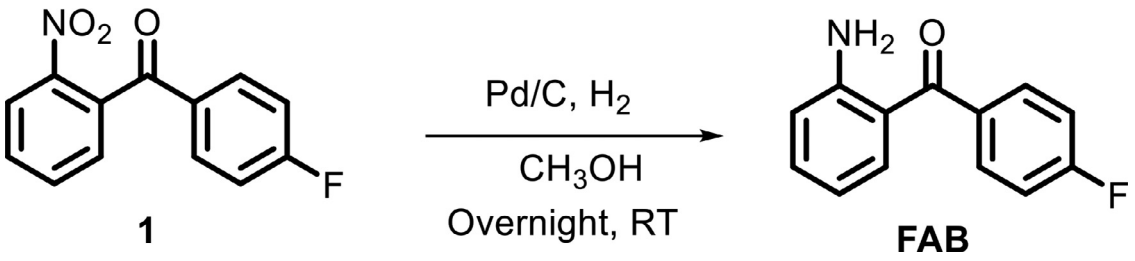


**Scheme 1.** Synthesis of molecule FAB.

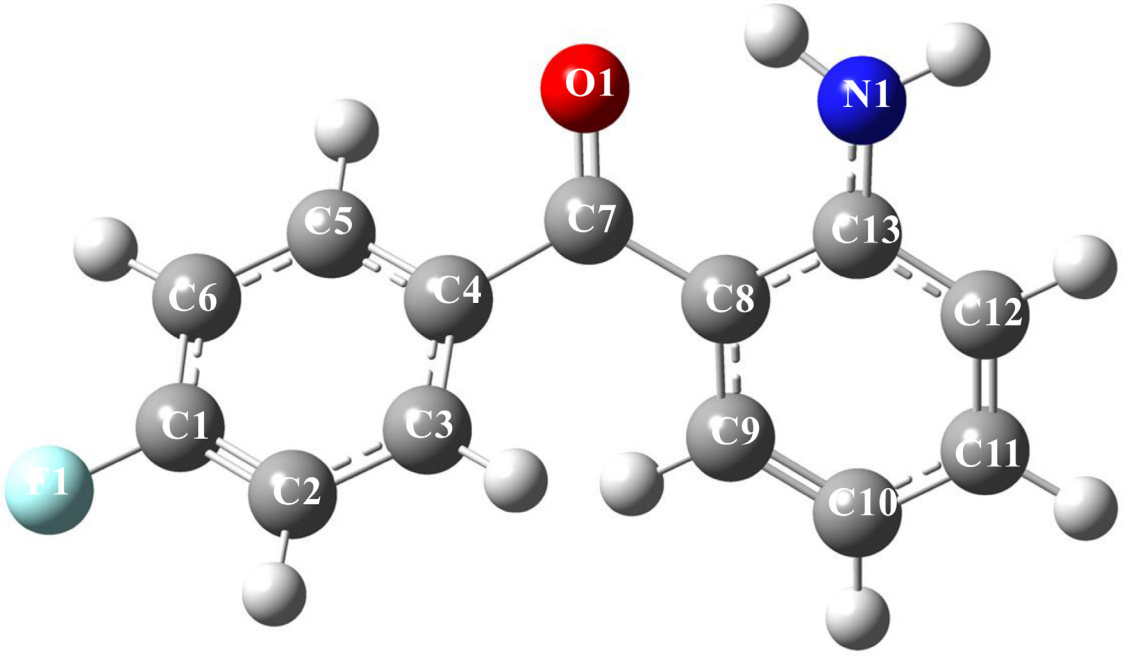


**Fig. 1.** Optimized structure of molecule FAB.

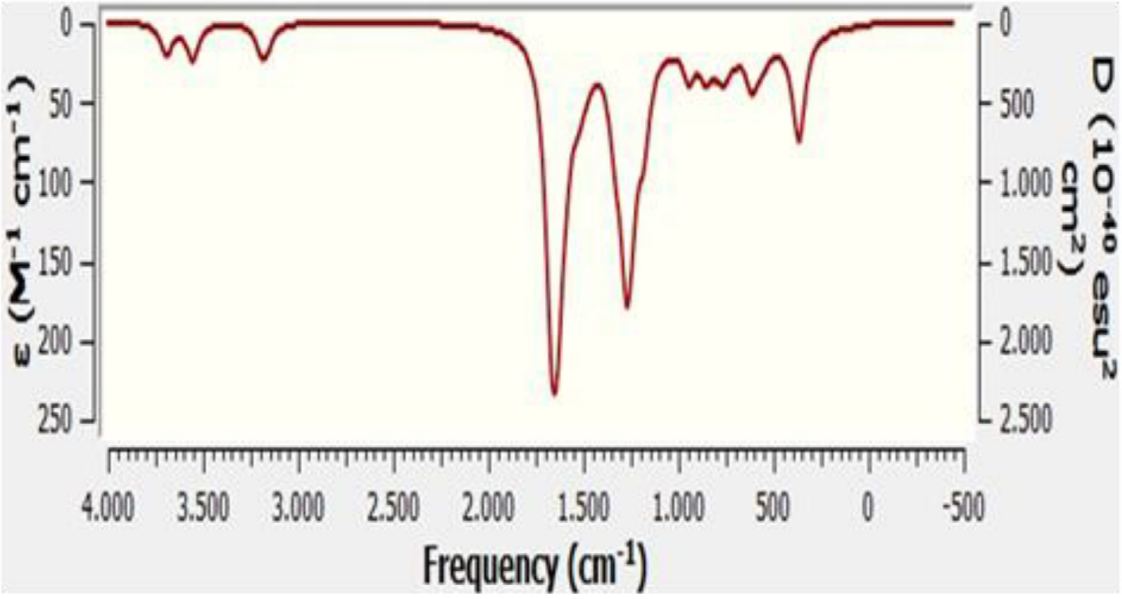


**Fig. 2.** The calculated IR spectrum of molecule FAB.

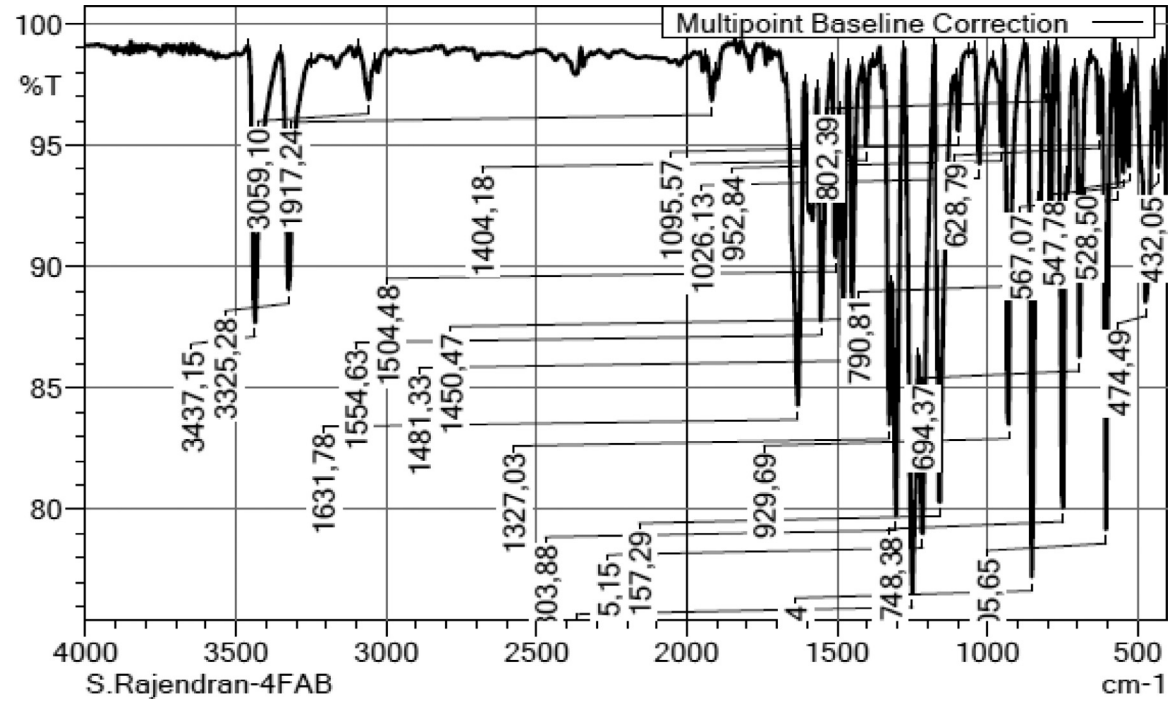


**Fig. 3.** FT-IR Spectrum of molecule FAB.

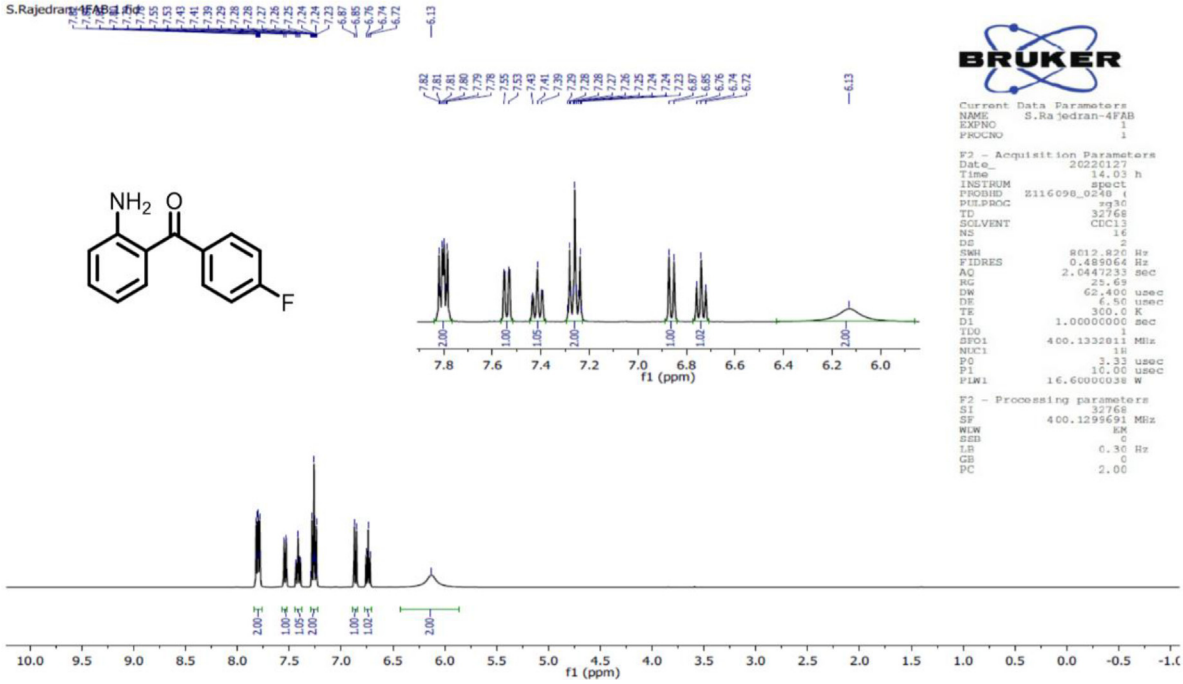


**Fig. 4.** $^{1}$H NMR spectrum of molecule FAB.

factor receptor 2 (VEGFR2). Further, the bioavailability of molecule (FAB) was investigated by ADME and p450 analyses.

## 2. Instrumentation methods

### *2.1. FT-IR and NMR analysis*

IR spectra (4000–400 $cm^{-1}$) were recorded with a (FT-IR) BRUKER VECTOR 22. $^{1}$H NMR and $^{13}$C NMR spectra was recorded on BRUKER AVANCE III HD-400 [400 MHz ($^{1}$H) and 100 MHz ($^{13}$C)] spectrometers using Tetramethyl silane (TMS) as an internal reference. The chemical shifts are expressed in parts per million (ppm). Coupling constants ($J$) are reported in hertz ($Hz$). The terms $J_o$ and $J_m$ refer to ortho coupling constant and meta coupling constant. The terms s, d, t, and dd refer to singlet, doublet, triplet, and doublet of doublet, respectively, and bs refers to a broad singlet. LC-MS experiments were carried out on an UHPLC Eksigent1 coupled with MS detector ABSciex1, Triple Quad 4500 model equipment. The samples were directly injected by using a syringe, and the data was collected in a range of 100.0–600.0 Da, at 200 Da $s^{-1}$ and positive polarity.

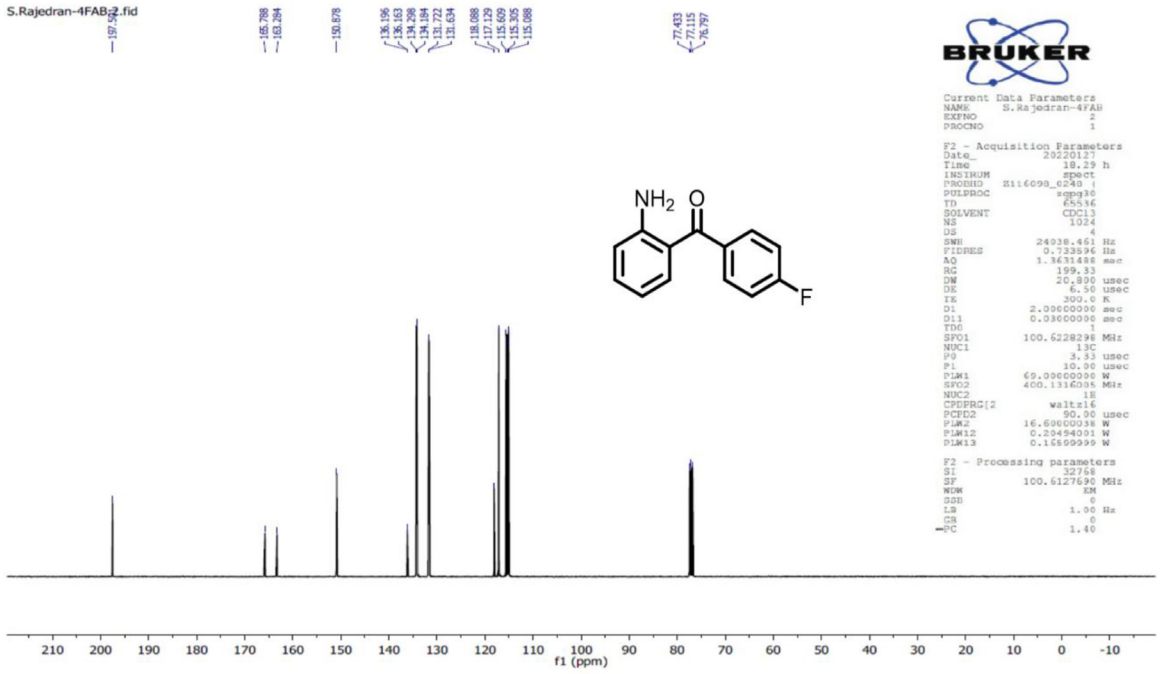


**Fig. 5.** $^{13}C$ NMR spectrum of molecule FAB.

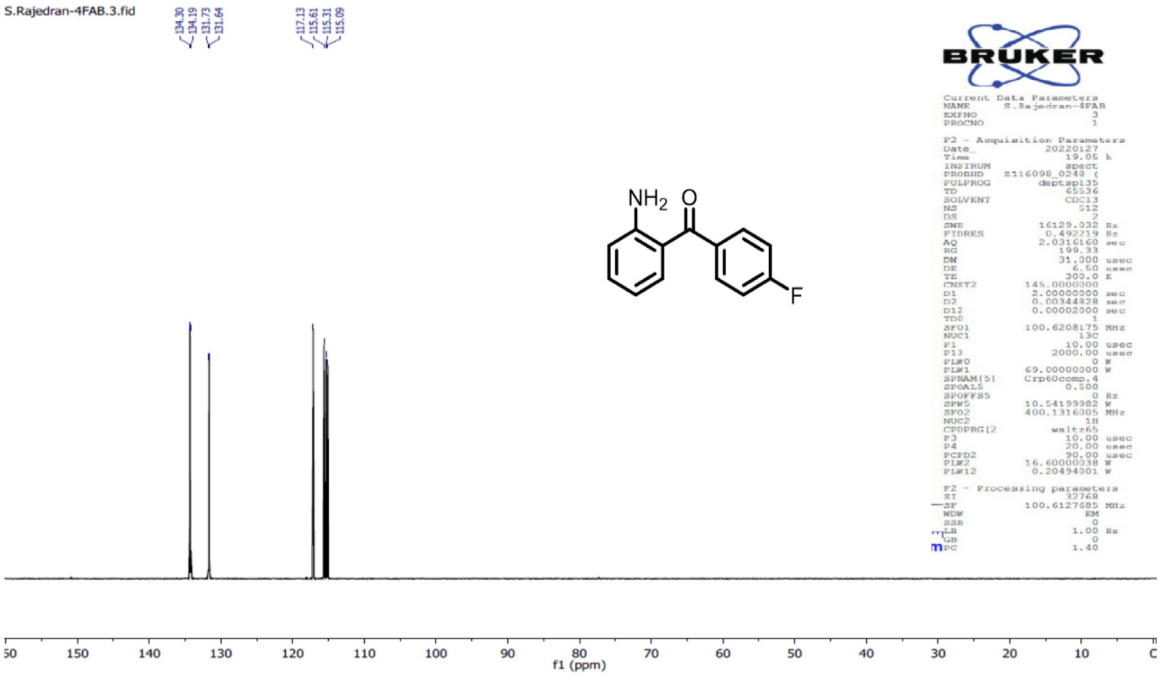


**Fig. 6.** DEPT 135 NMR spectrum of molecule FAB.

### 2.2. Single crystal XRD analysis

X-ray diffraction measurements were performed on a Bruker-Nonius FR590 Kappa CCD diffractometer at −173°C using monochromatic Mo-K$\alpha$ radiation.

### 2.3. DFT computational studies

Computational analyses of the studied compound were performed using Gaussian and Maestro 12.8 software [38–44]. Firstly, the studied compound was fully optimized at B3LYP/6-311+G(d) level in water phase. C-PCM solvent model was used to taken into consideration of solute-solvent interactions. Spectral calculations of it was performed at same level of theory. These calculations were done using Gaussian software.

As for the molecular docking analyses, the ligand and selected protein were minimized at pH=7 ± 2 using LigPrep and Protein Preperation modules, respectively. At these step, OPLS4 method was used in these calculations. Then, receptor binding domain of 3WZE was defined using Grid Generation module. Finally, molecular docking calculations were performed using Ligand Docking Module. Finally, ADME and p450 analyses are performed using same program which is Maestro Software 12.8.

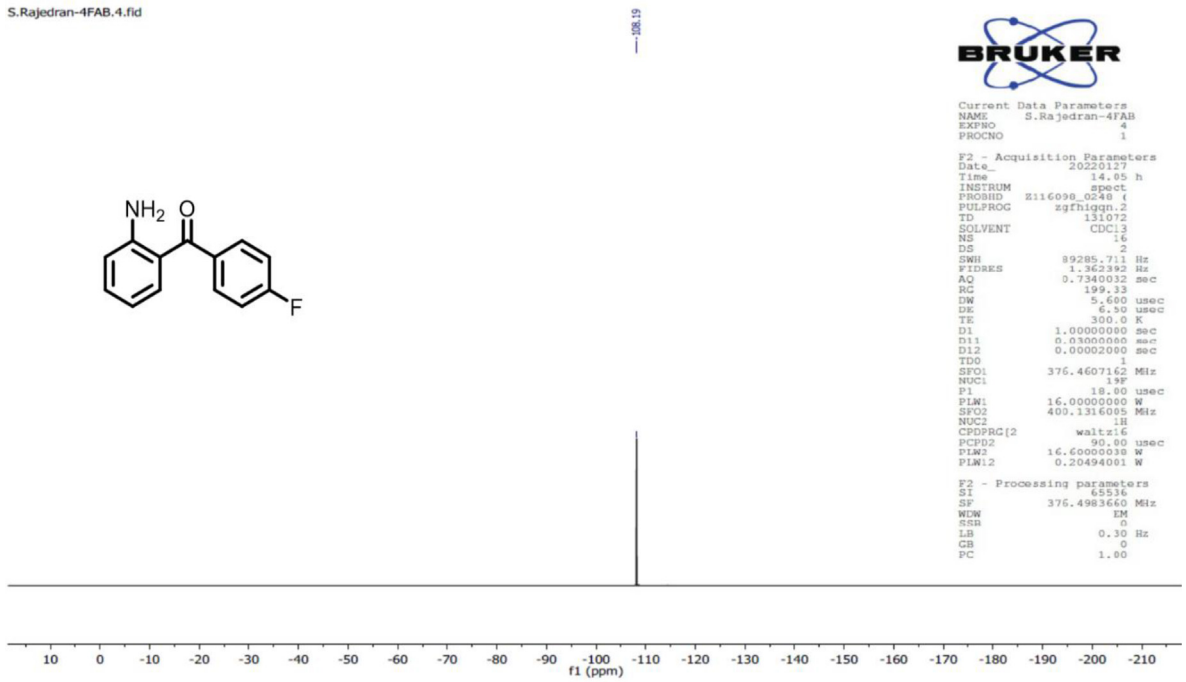


**Fig. 7.** $^{19}F$ NMR spectrum of molecule FAB.

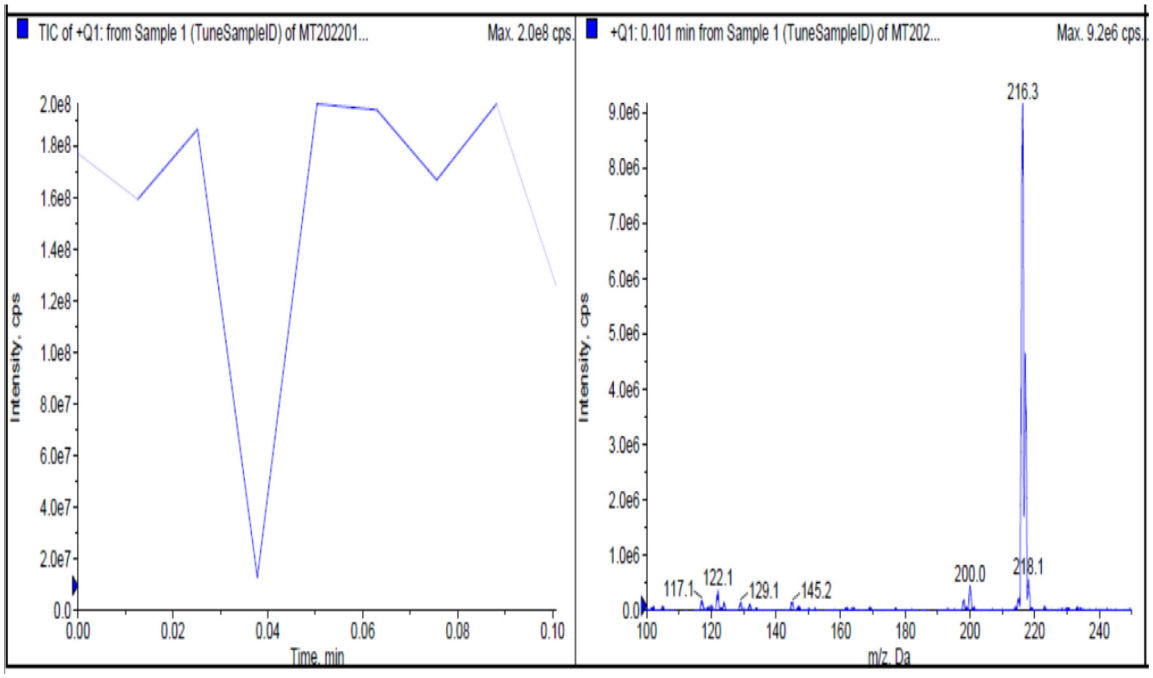


**Fig. 8.** LC-MS spectrum of molecule FAB.

## 3. Experimental details

### 3.1. General

All the reagents and chemicals were purchased from Sigma Aldrich and AKSci. Unless otherwise specified, other reagents were obtained from commercial suppliers. When known compounds had to be prepared according to literature procedures, pertinent references are given. The purity of the products was tested by TLC silica gel 60 F254 25 aluminum foil 20 × 20 C (purchased from Merck) using petroleum ether and ethyl acetate in the ratio of 95:5 as developing solvents. Melting points (M.p) were determined on a Kofler Thermogerate apparatus and were uncorrected. They are expressed in degree centigrade (°C).

### 3.2. Synthesis

#### 3.2.1. General procedure for preparation of 2-amino-4′-fluorobenzophenone (2)

A mixture of the 2-nitro-4′-fluorobenzophenone (**1,** 1 mmol) and Pd/C (0.005 mmol) was added under $H_2$ atm in presence methanol at RT for overnight. The completion of the reaction was

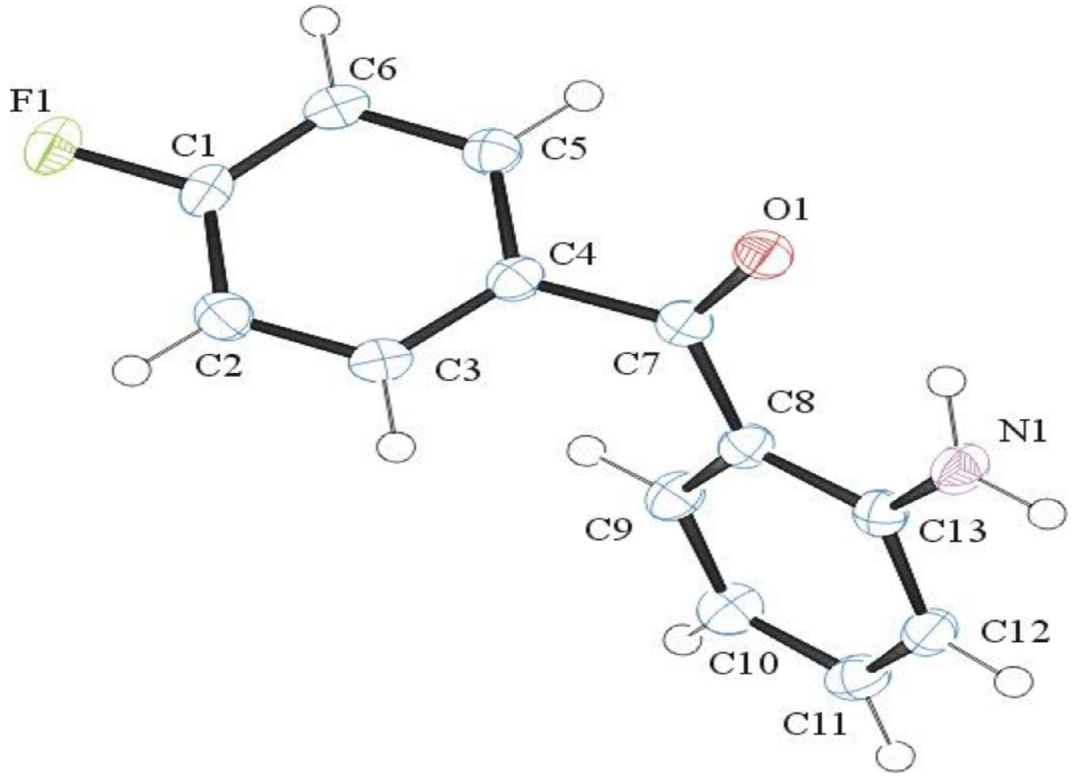


**Fig. 9.** ORTEP structure of the molecule FAB with thermal ellipsoids at the 50% probability level.

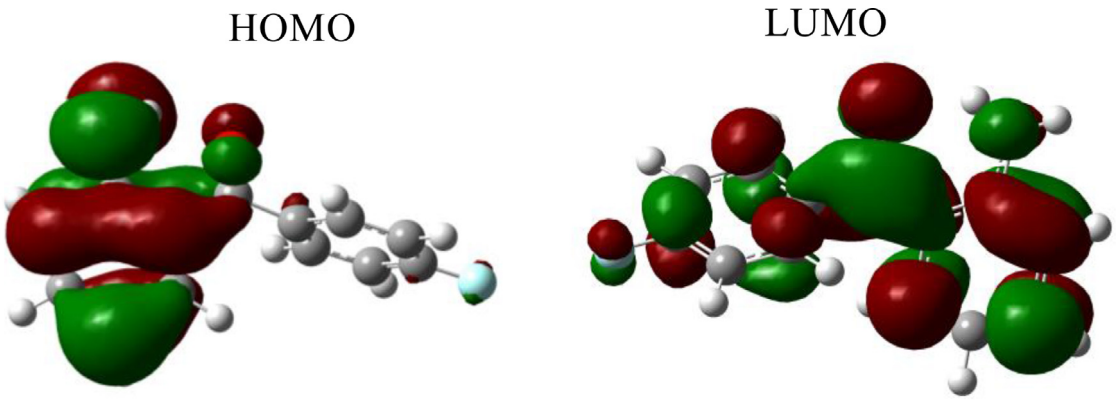


**Fig. 10.** Contour diagram of frontier molecular orbital of molecule FAB.

monitored by TLC. After stirring for overnight, the reaction mixture was filtered using celite and washed with EtOAc, then it was concentrated in vacuo to get FAB as a bright yellow solid. The obtained solid was recrystallized using EtOAc to afford a pure product of 2-amino-4′-fluorobenzophenone (FAB) crystals. Yield 92%, M.p 126–128°C (Lit. M.p[18–20] 127–128°C). $^{1}$H NMR (400 MHz, $CDCl_3$) (Fig. 5) (ppm) $\delta$: 6.13 (bs, 2H, N**H$_2$**), 6.74 (t, 1H, $C_{10}$-H, $J$ = 8.00 Hz), 6.86 (d, 1H, $C_{12}$-H, $J$ = 8.00 Hz), 7.23–7.29 (m, 2H, $C_2$, $C_6$ -H), 7.41 (t, 1H, $C_{11}$-H, $J$ = 8.00 Hz), 7.54 (d, 1H, $C_9$-H, $J$ = 8.00 Hz), 7.78–7.82 (m, 2H, $C_3$, $C_5$ -H); $^{13}$C NMR (100 MHz, $CDCl_3$) (Fig. 6) (ppm) $\delta$: 115.08 (t, $J_{C\text{-}F}$ = 21.7 Hz), 115.30 (t, $J_{C\text{-}F}$ = 21.7 Hz), 115.60, 117.12, 118.08, 131.63 (d, $J_{C\text{-}F}$ = 8.8 Hz), 131.72 (d, $J_{C\text{-}F}$ = 8.8 Hz), 134.18, 134.29, 136.16, 136.19 (d, $J_{C\text{-}F}$ = 3.3 Hz), 150.87, 163.28 (d, $J_{C\text{-}F}$ = 250.36 Hz), 197.50. $^{19}$F NMR (376 MHz, 298 K, $CDCl_3$) (Fig. 8) (ppm) $\delta$: −108.19. LC-MS (Fig. 9) for ($C_{13}H_{10}FNO$) $m/z$ (%) = 216.3 (M + 1, 100).

## 4. Results and discussion

### 4.1. Synthesis

The 2-nitro-4′-fluorobenzophenone (**1**) was treated with Pd/C under hydrogen atmosphere in the presence $CH_3OH$ at room temperature for overnight to yield 92% of 2-amino-4′-fluorobenzophenone (FAB) (Scheme 1) as a bright yellow solid.

### 4.2. Computational methods

#### 4.2.1. Fully optimizations

The studied compound is optimized at B3LYP/6-311+G(d) level in water. Molecular structure at ground state is given in Fig. 1.

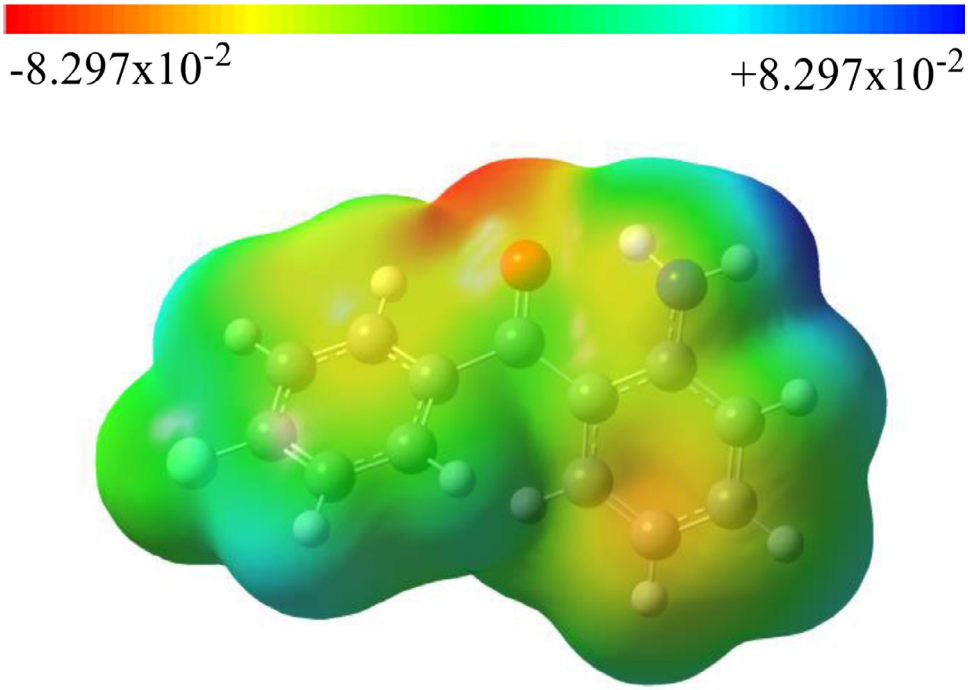


**Fig. 11.** Calculated MEP map of molecule FAB.

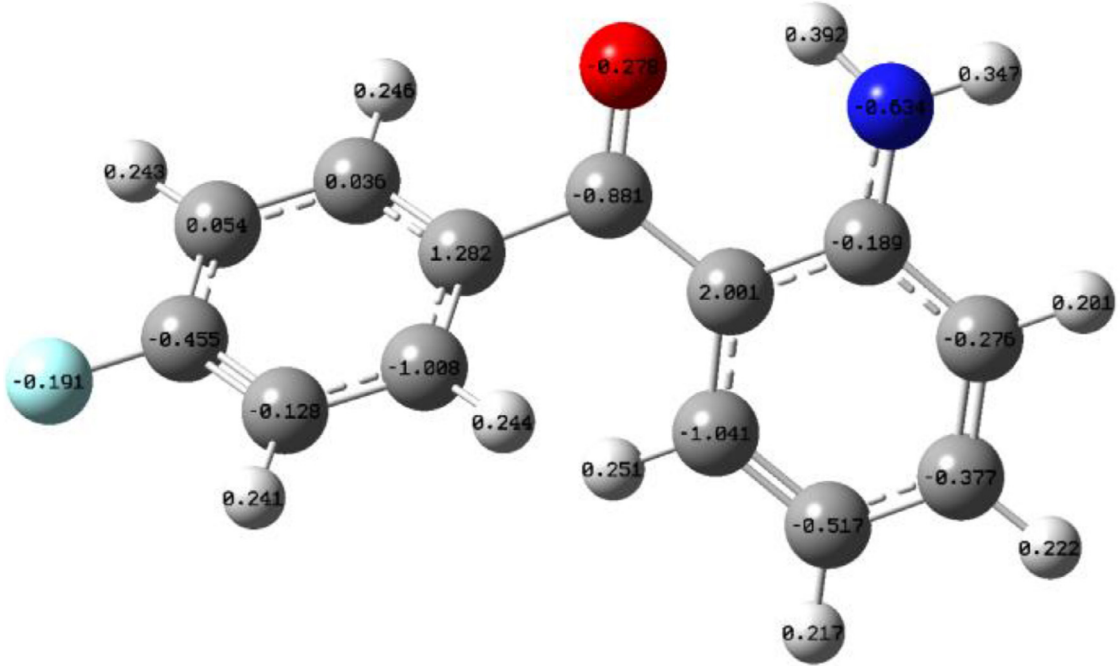


**Fig. 12.** Mulliken charge distribution of molecule FAB.

*4.2.2. FT-IR analysis*

FT-IR spectra are important for the characterization of molecule functional groups. The IR spectrum of molecule FAB was calculated using B3LYP/6-311+G(d) level in water and represented in Fig. 2. Calculated and experimental harmonic stretching frequencies are given in Table 1. The major characteristic peaks of symmetric and asymmetric stretching of molecule FAB in the FT-IR (KBr, cm-1) spectrum (Fig. 3), due to $NH_2$ functional group are, found at 3437 $cm^{-1}$ and 3325 $cm^{-1}$, respectively. The other characteristic groups, i.e. C=O stretching is found at 1631 $cm^{-1}$ and C=N stretching at 1554 $cm^{-1}$. The theoretical values of FT-IR, which is given by B3LYP/6-311+G(d) (Fig. 2) levels of theory are mostly in good agreement, Table 1.

*4.2.3. FT-NMR analysis*

$^{1}H$ NMR (400 MHz) and $^{13}C$ NMR (100 MHz) spectra were recorded in $CDCl_3$ using TMS as the internal standard. $^{1}H$ NMR and $^{13}C$ NMR chemical shifts of FAB are given in Table 2. Within the $^{1}H$ NMR (Fig. 4), the $NH_2$ protons peaks were observed in the downfield region at $\delta$ 6.13 as a broad singlet. The rest of aromatic protons appeare in the region between $\delta$ 6.86–7.82. The $^{13}C$ NMR spectrum shows the presence of 13 carbons. The characteristic sig-

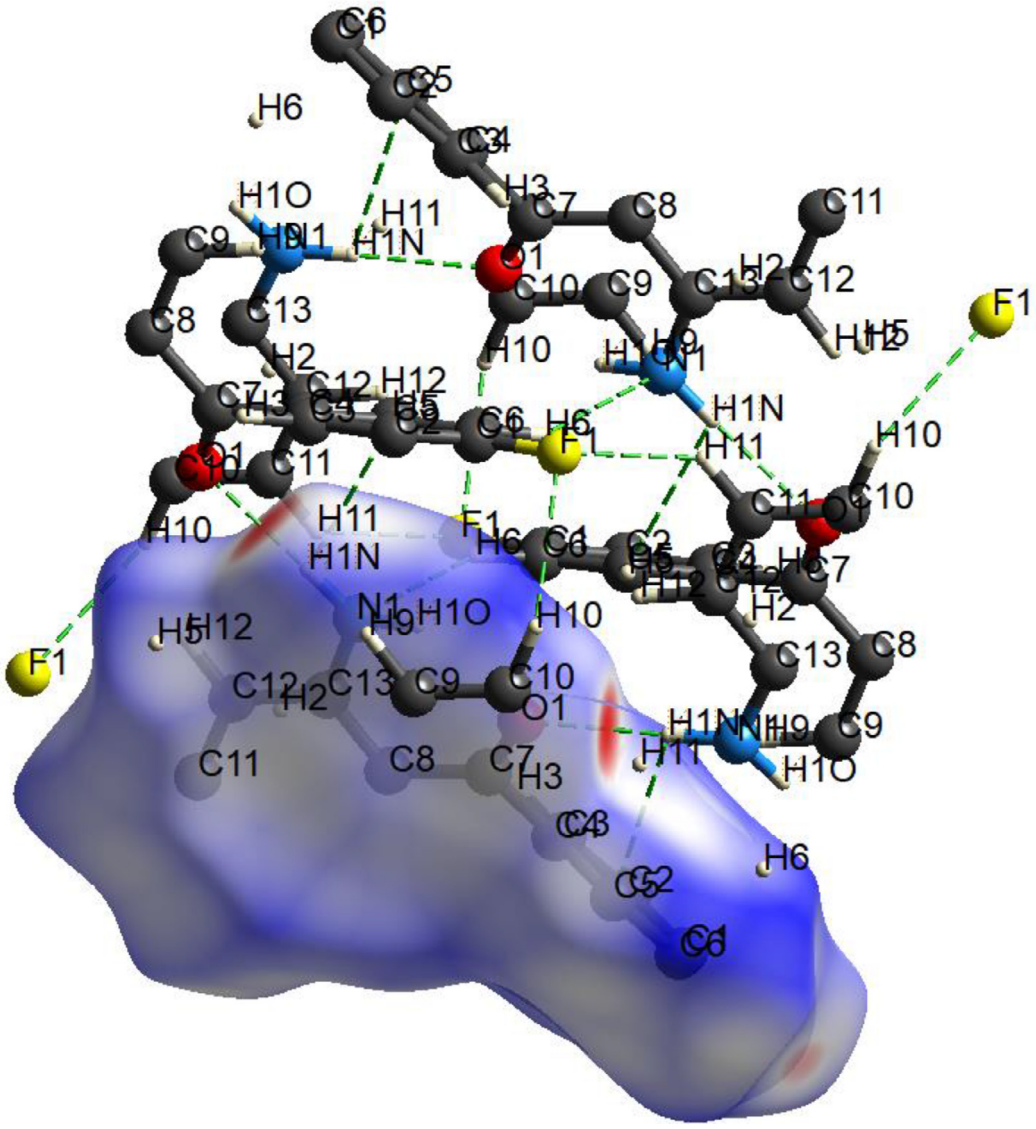


**Fig. 13.** The bright red spot on the hirshfeld surface correspond to donor and acceptor atoms involved in van der Waals interactions of FAB. (For interpretation of the references to color in this figure legend, the reader is referred to the web version of this article.).

**Table 1**
FT-IR frequencies ($cm^{-1}$) (Figs. 2 and 3).

| Assignments | Experimental | B3LYP/6-311+G(d) |
|---|---|---|
| $\nu_{NH\ asymmetric}$ | 3437 | 3692 |
| $\nu_{NH\ symmetric}$ | 3325 | |
| $\nu_{CH}$ | 3059 | 3188 |
| $\nu_{C=O}$ | 1631 | 1681 |
| $\nu_{C-N}$ | 1554 | 1664 |
| $\nu_{C=C}$ | 1504 | 1625 |
| $\nu_{C-F}$ | 1249 | 1245 |

nal at $\delta$ 197.50 is due to $-C_7=O$ (Fig. 5). The C-F site carbon atom was found at $\delta$ 163.28 (d, $J_{C-F}$ = 250.36 Hz), Fig. 5. All other aromatic carbons appeare in the region of $\delta$ 115.08–150.87. The characteristic peak at $\delta$ −108.19 in $^{19}F$ NMR spectra is due to the fluorine atom (Fig. 7). Furthermore, the DEPT-135 spectra (Fig. 6) and LC-MS (Fig. 8) were in good agreement with the proposed molecular formula $C_{13}H_{10}FNO$.

The $^1H$ and $^{13}C$ NMR spectra of molecule FAB was calculated by using B3LYP/6-311+G(d) level in water and the theoretical $^1H$ and $^{13}C$ chemical shift values compared with experimental $^1H$ and $^{13}C$ chemical shift values showed in Table 2. The theoretical $^1H$ and $^{13}C$ chemical shift results for molecule FAB are mostly closer to the experimental $^1H$ and $^{13}C$ shift data.

*4.2.4. Single crystal XRD studies*

*4.2.4.1. Crystal and molecular structure.* A colorless block, measuring 0.50 × 0.30 × 0.10 $mm^3$ was mounted on a loop with oil. Data was collected at −173 °C on a Nonius Kappa CCD FR590 single crystal X-ray diffractometer, Mo-K$\alpha$ radiation. Crystal-to-detector distance was 40 mm and exposure time was 60 s per degree for all sets. The scan width was 2°. Data collection was 99.9% complete to 25° in ϑ. A total of 38,149 partial and complete reflections were collected covering the indices, −11<=*h*<=11, −14<=*k*<=14, −13<=*l*<=13. A total of 4813 merged and 2482 symmetry independent reflections with $R_{int}$ = 0.0358 were collected. Indexing and unit cell refinement indicated a triclinic lattice. The space group was found to be $P2_1/a$ (No. 14). The data was integrated and scaled using hkl-SCALEPACK [45]. Solution by direct methods (SHELXT [46] or SIR97 [47,48]) produced a complete heavy atom phasing model consistent with the proposed structure. The structure was completed by difference Fourier synthesis with

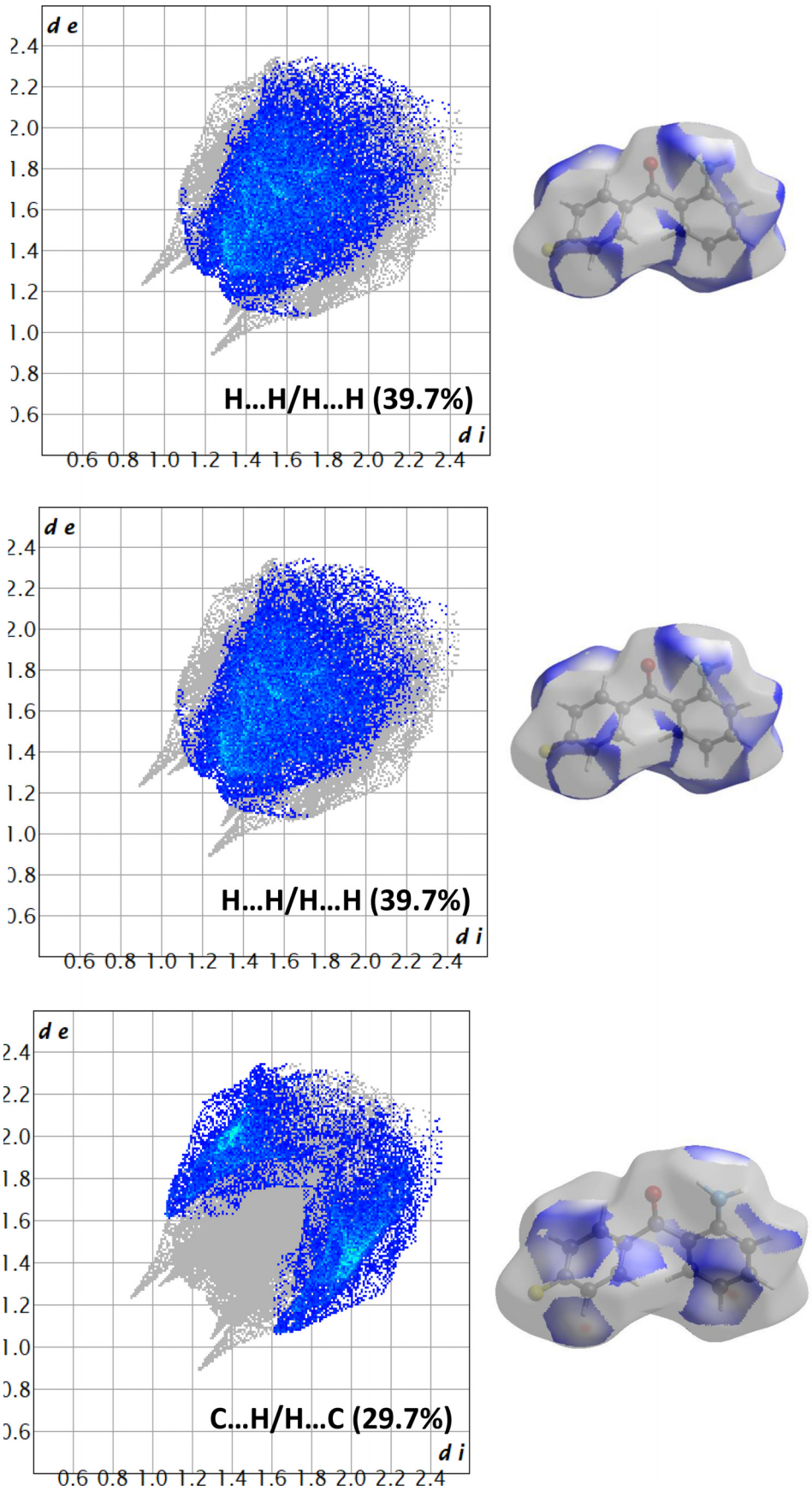


**Fig. 14.** 2D Finger plots with corresponding Hirsfeld surface of the FAB calculated based on $d_{norm}$.

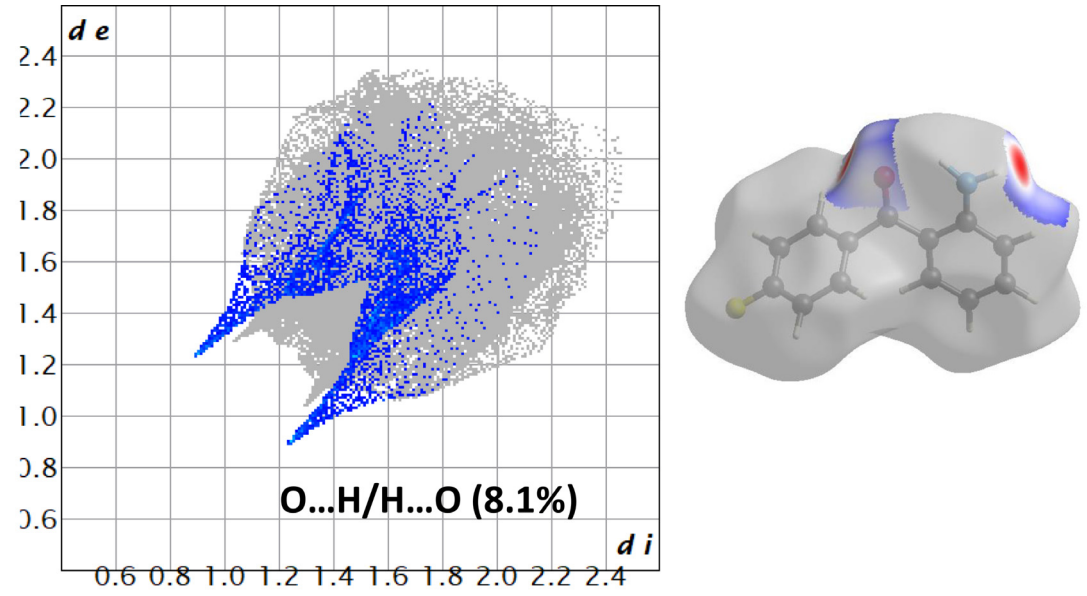


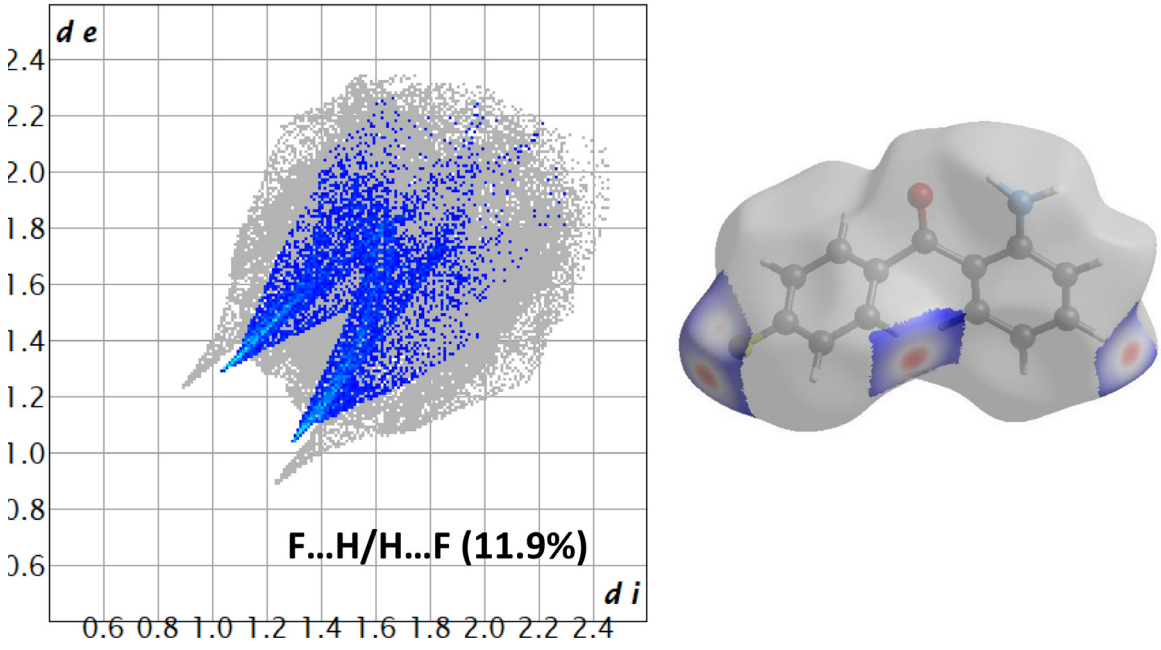


**Fig. 14.** Continued

**Table 2**
$^{1}$H and $^{13}$C NMR Chemical shift $\delta$ (ppm) (Figs. 5–9).

| Atoms | $^{1}$H NMR | | Atoms | $^{13}$C NMR | |
|---|---|---|---|---|---|
| | Experimental | B3LYP/6-311+G(d) | | Experimental | B3LYP/6-311+G(d) |
| N1H | 6.13 | 7.6 | C1 | 136.16 | 137.9 |
| C1H | 7.41 | 7.6 | C2 | 115.6 | 118.2 |
| C2H | 6.86 | 7 | C3 | 150.87 | 175.1 |
| C5H | 7.54 | 8.1 | C4 | 117.12 | 118.6 |
| C6H | 6.74 | 7.2 | C5 | 134.18 | 139 |
| C9H | 7.23–7.29 | 7.2 | C6 | 118.08 | 121.1 |
| C10H | 7.78–7.82 | 7.5 | C7 | 197.5 | 203.8 |
| C11H | 7.78–7.82 | 7.3 | C8 | 115.3 | 123.8 |
| C12H | 7.23–7.29 | 6.6 | C9 | 131.72 | 140.8 |
| | | | C10 | 134.29 | 144.2 |
| | | | C11 | 131.61 | 139.7 |
| | | | C12 | 115.08 | 119.9 |
| | | | C13 | 163.28 | 159.8 |

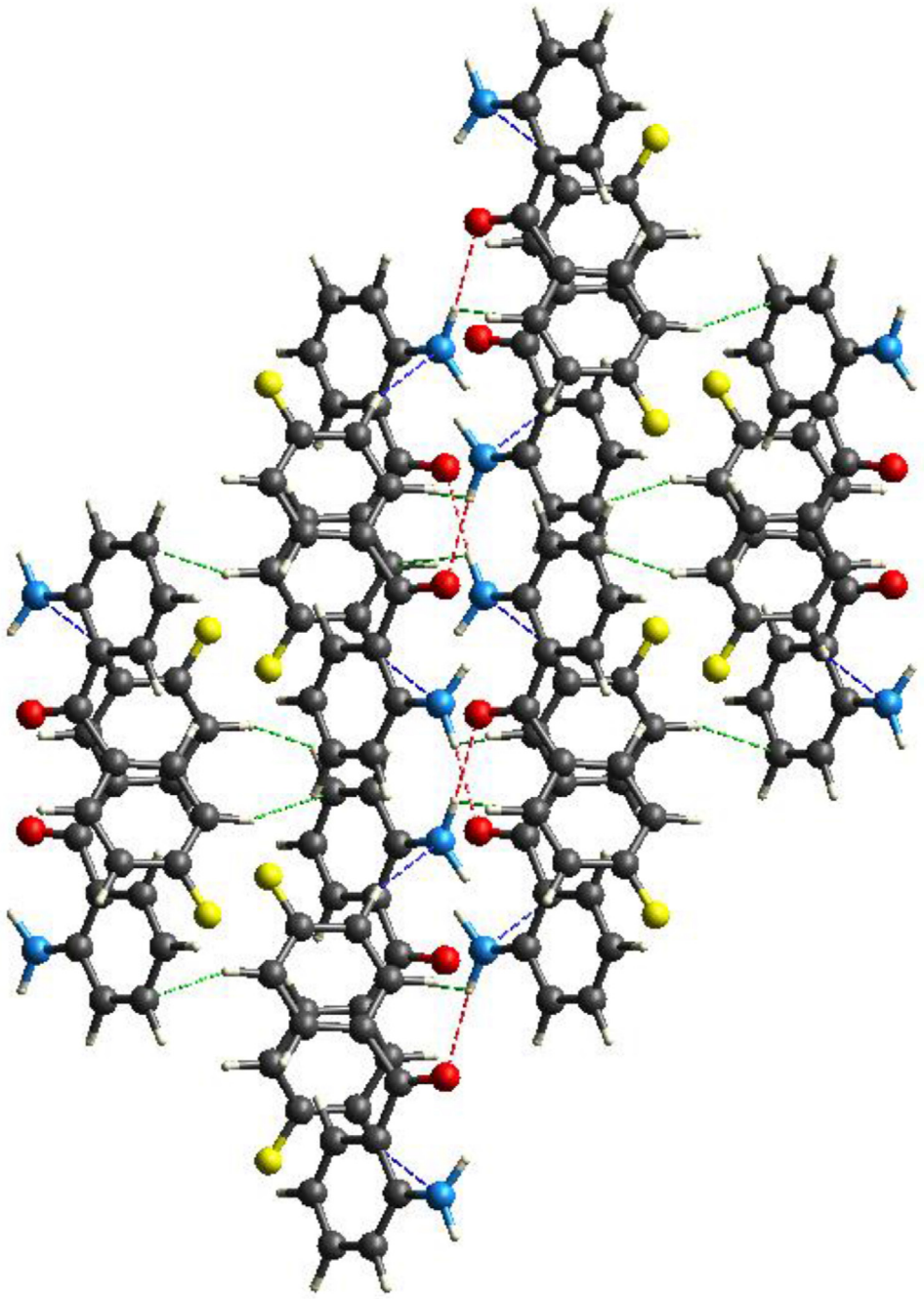

**Fig. 15.** Partial Packing diagram of FAB viewed along *a* axis of the unit cell with C…H (green), N…H(blue) and O…H (red) hydrogen bonds. (For interpretation of the references to color in this figure legend, the reader is referred to the web version of this article.).

SHELXL [49,50], Scattering factors are from Waasmair and Kirfel [51]. Hydrogen atoms were placed in geometrically idealized positions and constrained to ride on their parent atoms with C—H distances in the range 0.95–1.00 Angstrom. Isotropic thermal parameters $U_{eq}$ were fixed such that they were $1.2U_{eq}$ of their parent atom Ueq for CH's and $1.5U_{eq}$ of their parent atom $U_{eq}$ in case of methyl groups. All non-hydrogen atoms were refined anisotropically by full-matrix least-squares. Table 3 summarizes the data collection details. Fig. 9 shows an ORTEP [52] of the asymmetric unit.

Calculated geometrical parameters (Bond length, Bond Angle and Dihedral angle) of molecule FAB and single crystal XRD data are listed in Table 4, following atom numbering scheme given in Fig. 1.

*4.2.5. Frontier molecular orbitals (FMOs), MEP maps and MEP contours*

Significant electronic properties of a compound can be determined from contour plots of frontier molecular orbital and molecular electrostatic potential (MEP) map. The highest occupied molecular orbital (HOMO) and the lowest unoccupied molecular orbital (LUMO) are represented in Fig. 10.

HOMO electrons are mainly delocalized on the $NH_2$ substituted side of the compound while the whole structure is seen as active in the LUMO diagram. Especially, $\pi$ electrons are seen to a play significant role in the activation of the molecule. The MEP map is represented in Fig. 11.

Red color in the MEP map, Fig. 11, implies the electron-rich region while dark blue shows the electron-poor region. Specifically,

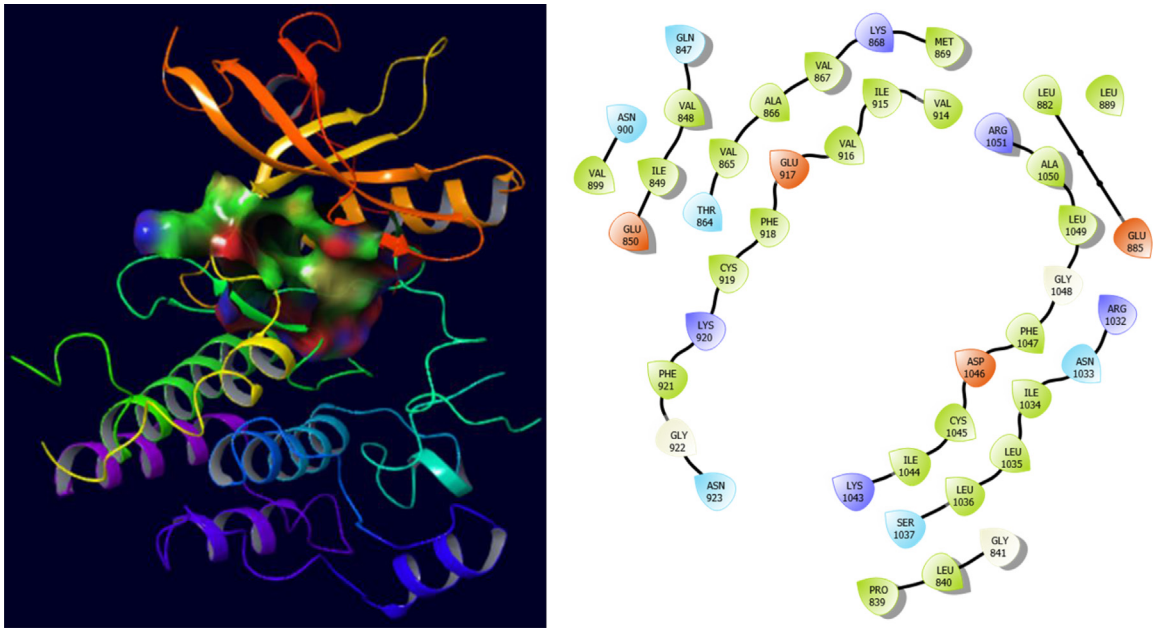


**Fig. 16.** The electrostatic potential map of receptor binding site of the target protein.

**Table 3**
Crystallographic data for the structure of molecule FAB.

| | |
|---|---|
| CCDC Number | 2144792 |
| Empirical formula | $C_{13}H_{10}FNO$ |
| Formula weight | 215.22 |
| Temperature | 100(2) K |
| Wavelength | 0.71073 Å |
| Crystal system | Monoclinic |
| Space group | $P2_{1/a}$ |
| Unit cell dimensions | $a$ = 8.8411(3) Å $\alpha$= 90°<br>$b$ = 11.2131(4) Å $\beta$= 100.045(2)°<br>$c$ = 10.3465(5) Å $\gamma$ = 90° |
| Volume | 1009.99(7) Å3 |
| Z | 4 |
| Density (calculated) | 1.415 Mg/m$^3$ |
| Absorption coefficient | 0.103 mm$^{-1}$ |
| F(000) | 448 |
| Crystal size | 0.500 × 0.300 × 0.100 mm$^3$ |
| Theta range for data collection | 1.999 to 28.235° |
| Index ranges | −11<=$h$<=11,<br>−14<=$k$<=14,<br>−13<=$l$<=13 |
| Reflections collected | 4813 |
| Independent reflections | 2482 [R(int) = 0.0358] |
| Completeness to theta = 25.000° | 99.9% |
| Refinement method | Full-matrix least-squares on F2 |
| Data / restraints / parameters | 2482 / 0 / 153 |
| Goodness-of-fit on F$^2$ | 1.085 |
| Final R indices [$I$>2sigma(I)] | R1 = 0.0397, wR2 = 0.0994 |
| R indices (all data) | R1 = 0.0589, wR2 = 0.1064 |
| Largest diff. peak and hole | 0.317 and −0.182 e.Å$^{-3}$ |

the oxygen atom is appropriate for nucleophilic attack which increases the reactivity of FAB.

#### 4.2.6. Mulliken charges

Mulliken charges, indicative of active sites in FAB are represented in Fig. 12.

According to Fig. 12, heteroatoms are seen as negative except the fluorine atom. Its electronic charge is too low. Carbon atoms C2, C3, C4, C5, C11 and C13 have negative charge and can be reactive. Considering the steric hindrance, only C2, C3 and C4 reactivity can be considered high.

**Table 4**
The geometric parameters of molecule FAB at B3LYP/6-311+G(d) level.

| Bond Angle (deg.) | | Dihedral Angle (deg.) | | Bond Lengths (Å) | |
|---|---|---|---|---|---|
| C4-C7-C8 | 120.3 | C5-C4-C7-C8 | −144.3 | C1-F1 | 1.353 |
| C6-C1-F1 | 118.8 | C10-C11-C12-C13 | −0.05 | C7-C8 | 1.478 |
| C7-C8-C13 | 120.6 | C11-C12-C13-N1 | −179.8 | C7-O1 | 1.232 |
| C8-C7-O1 | 121.8 | O1-C7-C8-C13 | 18.6 | C12-C13 | 1.411 |
| C11-C12-C13 | 121.3 | F1-C1-C6-C5 | 179.4 | C13-N1 | 1.366 |
| C12-C13-N1 | 119.5 | | | | |

#### 4.2.7. Hirshfeld surface analysis

To quantify the intermolecular interactions within the crystal structure, the Hirshfeld and 2D finger plot analysis was carried out using Crystal Explorer [53]. The bright red spot on the Hirshfeld surface indicates the acceptor and donor atoms involved in non-bonding interactions such as O1-H1…N1, N1-H…O1, F1-H10…C10, C5…H1-N1, N1…H6-C6, N1-H1…C5, C10-H10…F1 (Fig. 13). These results are also substantiated in the MEP map of the compound where the negative potential (acceptor) as red surface around O1 and the positive potential (donor) as green surface around N1 and F1. Most prominent inter molecular interactions are shown in Fig. 14. The 2D Fingerprint plot shows H-H interactions appear largely as 39.7% with a high concentration at $d_e$=$d_i$=1.8 Å. The C…H/H…C contacts contribute to 29.7% appeared as two spikes in the vicinity of $d_e$+$d_i$~2 Å. F…H/H…F contacts contribute to 11.9% of the Hirshfeld area. All other contacts contributed less than 10%. Thus, C…H/H…C contacts dominate the crystal packing (Fig. 15) of FAB.

### 4.3. Molecular docking and ADME studies

The molecular docking method is used to study the interactions of chemical species with biological macromolecules. Molecular docking plays a significant role in the development of a potential drug by conveying a variety of biological information. For this goal, the target protein 3WZE, a is vascular endothelial growth factor receptor 2 (VEGFR2), was studied at pH=7 ± 2 with the OPLS4 method. The electrostatic potential maps of receptor binding domain (RBD) and significant amino acids in the RBD is represented in Fig. 16.

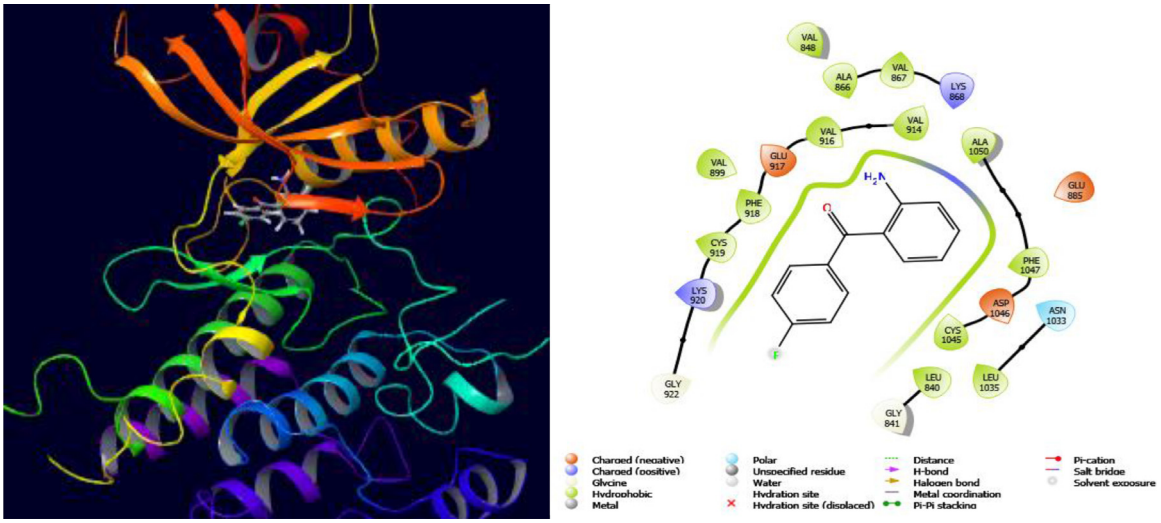


**Fig. 17.** The docking structure and interaction map between molecule FAB and 3WZE.

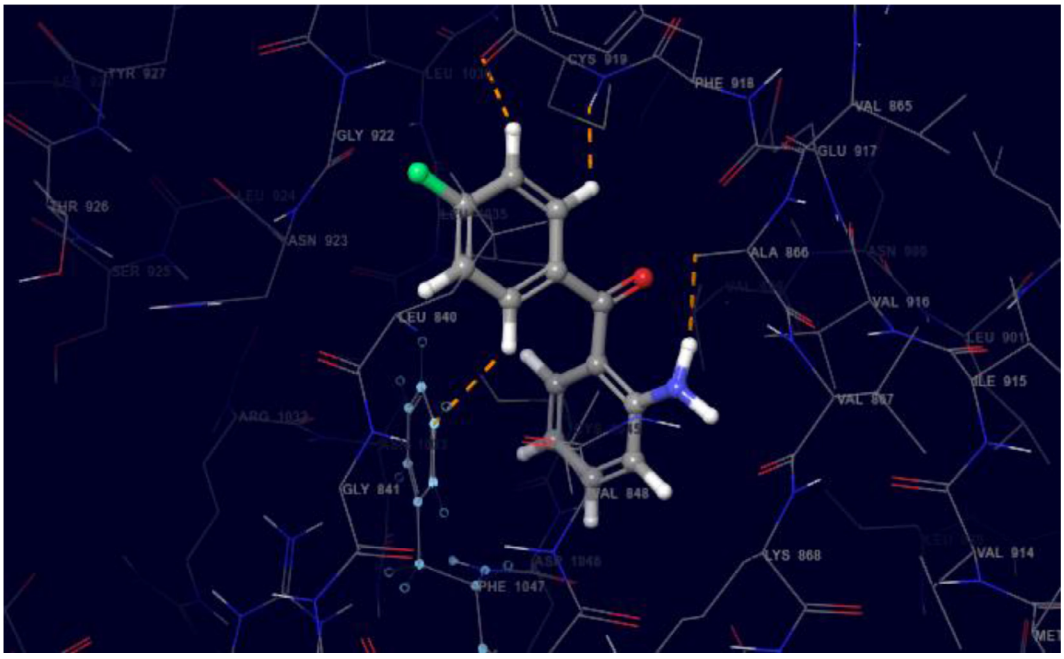


**Fig. 18.** The interactions between FAB and RBD of 3WZE.

According to Fig. 16, there are different colours and there is a mean for each of them. Actually, these colours imply the electron densities. The most electron density is showing with red color while the most positive site is representing with dark blue color. Additionally, significant amino acids chains are represented in revised manuscript. These amino acids have potential to interact with molecules. Molecular docking calculations are performed between studied compound and target protein. Docking score, van der Waals energy, coulomb energy and total interaction energy are calculated as −6.92, −28.21, −0.64 and −28.85, respectively. The docking structure and interaction map are represented in Fig. 17.

According to Fig. 17 and molecular docking results, the key-lock harmony between ligand and protein is surveyed as −6.92 kcal/mol and the interaction energy is calculated as −28.85 kcal/mol. These values imply that FAB is in good interaction with 3WZE in complex structure. Furthermore, interaction types between FAB and 3WZE are indicated in Fig. 17, too. The dominant interaction types are hydrophobic, charged (negative), charged (positive) and polar. Finally, solvent exposure is observed. The interactions between FAB and 3WZE are represented in more detail in Fig. 18.

According to Fig. 18, FAB interacts badly with ALA866, PHE1047 and CYC919 while it interact better with the other amino acids. VEGFR2 is highly effective in both growth and nutrition of cancer cells. Inhibiting this target will not only slow down the growth of the cancer cell, but will also try to prevent proliferation. Due to the fact that inhibition of VEGFR2 is vital in the treatment and prevention of cancer. According to obtained results, VEGFR2 can be inhibited by FAB molecule. Pharmacokinetic and pharmacology analyses of studied compound is investigated using 'Absorption, Distribution, Metabolism, and Excretion' (ADME) and p450 calculations. These analyses are done for the molecule FAB. ADME results are given in Table 5.

According to Table 5, ADME properties of studied molecule FAB appear well within recommended values for docking, demonstrating the potential to be a drug. p450 analyses are done in detail to study FAB affinity towards CYP2C9 and CYP3A4 enzymes, see Fig. 17.

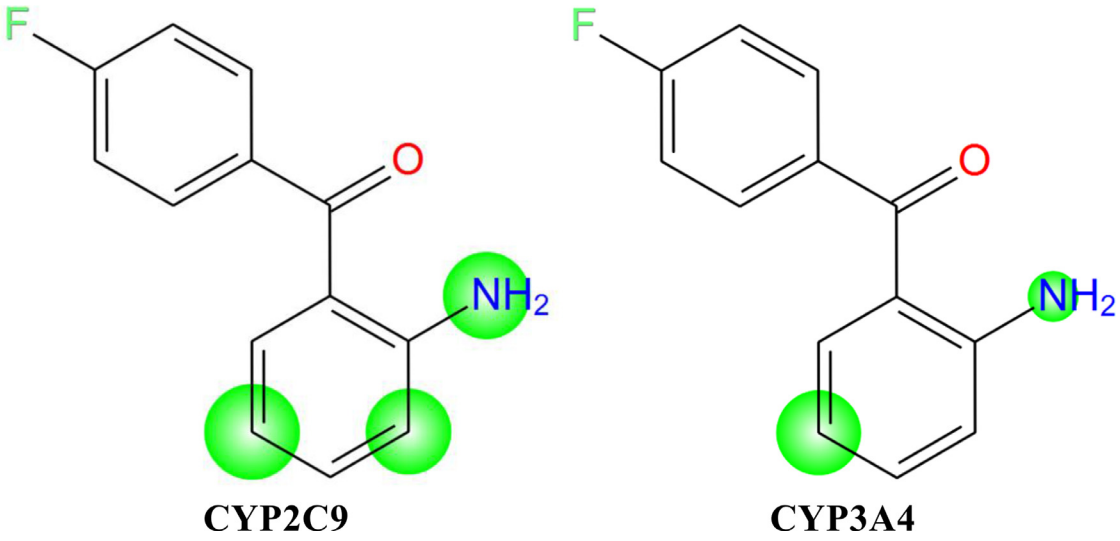


**Fig. 19.** Molecular reactivity against CYP2C9 (a) and CYP3A4 (b).

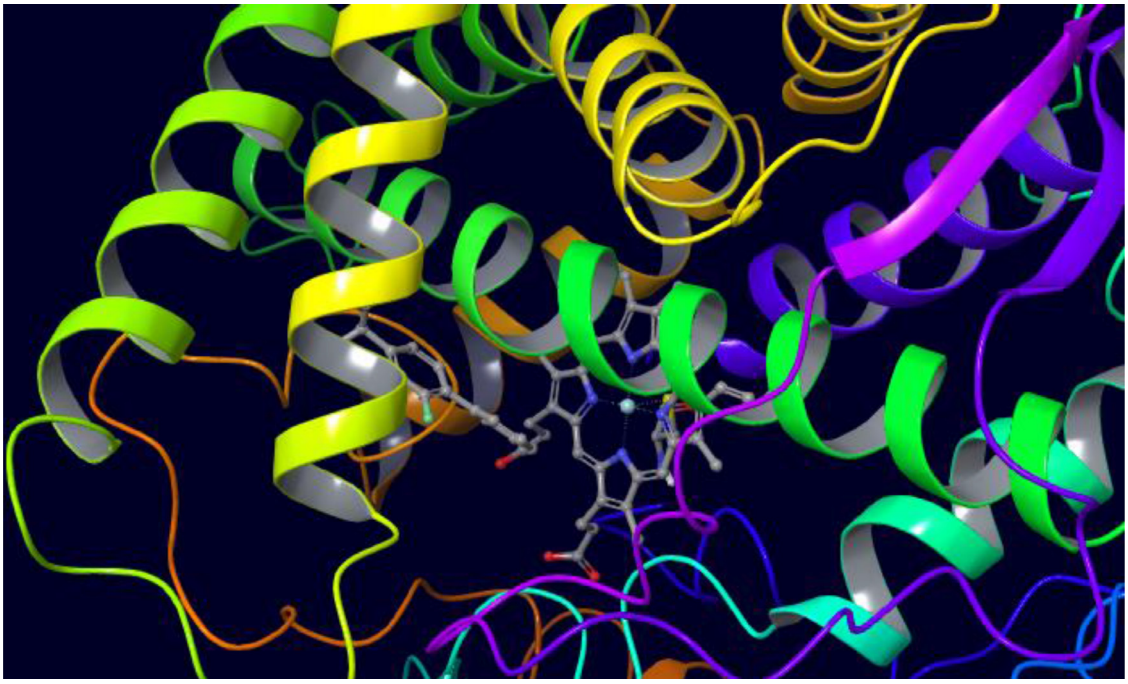

**Fig. 20.** The complex structure between molecule FAB and CYP2C9.

**Table 5**
ADME results of studied compound.

| Descriptors | Calculated | Recommended | Descriptors | Calculated | Recommended |
|---|---|---|---|---|---|
| #stars | 0 | 0 – 5 | mol_MW | 215.226 | 130 – 725 |
| #amine | 0 | 0 – 1 | PISA | 303.331 | 0 – 450 |
| #acid | 0 | 0 – 1 | donorHB | 1 | 0 – 6 |
| #rotor | 3 | 0 – 15 | accptHB | 2 | 2 – 20 |
| #rtvFG | 0 | 0 – 2 | QPpolrz | 23.453 | 13 – 70 |
| CNS | 0 | −2 to +2 | QPlogBB | −0.248 | −3.0 – 1.2 |
| QPPMDCK | 1353.6 | <25 poor, > 500 great | #metab | 2 | 1 – 8 |
| QPlogKp | −1.774 | −8 – −1 | PSA | 49.615 | 7.0 – 200.0 |
| #NandO | 2 | 2 – 15 | RuleOfFive | 0 | Max. 4 |
| RuleOfThree | 0 | Max. 3 | #noncon | 0 | – |
| Jm | 2.119 | – | #in56 | 12 | – |

Indicated in Fig. 19 are active sites for 2C9 in FAB that can interact with CYP enzyme. The color of circles indicates the sites that will interact with the CYP enzyme, while the size of the circles is directly proportional to the willingness to interact. Based on this result, the investigated compound seems more likely to interact with CYP2C9. It seems that FAB inhibit the CYP2C9 while less likely CYP3A4. The complex structure between studied molecule FAB and CYP2C9 is represented in Fig. 20.

As a result, the studied molecule FAB is predicted to act as an inhibitor of CYP2C9. Since this situation is undesirable, a future drug dose adjustment study may be able to mitigate this behavior. The bioavailability of the studied molecule FAB can be seen at an acceptable level. Because it is known that CYP3A4 is responsible for the metabolism of 50% of the drugs taken into the body.

## 5. Conclusion

The synthesis and crystal structure of molecule 2-amino-4′-fluorobenzophenone (FAB) is identified by using FT-IR, $^{1}H$ and $^{13}C$ NMR chemical shifts, the results of which compare well with calculated parameters using B3LYP/ 6-311+G(d) basis sets in water. The theoretical values of FT-IR, $^{1}H$ and $^{13}C$ NMR chemical shifts, which is given by B3LYP/6-311+G(d) levels of theory are mostly in good agreement with experimental values. The optimized geometry of the molecule (FAB) was compared to the experimental XRD values. DFT calculations of the molecular electrostatic potential (MEP), frontier molecular orbitals (FMO), Hirshfeld surface analysis and Mulliken charges recognize the chemically active sites of this molecule responsible for its chemical reactivity. Mainly, the HOMO electrons are delocalized on the $NH_2$ substituted side of the compound while the whole structure is seen as active in the LUMO diagram. Especially, $\pi$ electrons are seen to a play significant role in the activation of the molecule FAB. *In silico* molecular docking analyses indicates FAB docking on vascular endothelial growth factor receptor 2 (VEGFR2) (PDB: 3WZE) kinase inhibitors. Further, the bioavailability through ADME and p450 analyses of FAB indicates inhibitor of the CYP2C9 enzyme, however FAB may have a high potential to be a drug in the medicinal applications. The molecule FAB is a potential starting precursor for many biologically active heterocyclic analogues for our future works.

## Supplementary data

CIF files for compounds **2** have been deposited with the Cambridge Crystallographic Data centre as CCDC number 2144792. Copies of the data can be obtained, free of charge, on application to CCDC, 12 Union Road, Cambridge, CB2 1EZ, UK. Fax: +44 (0) 1223 336033 or email: deposit@ccdc.cam.ac.uk.

## Declaration of Competing Interest

The authors are aware of its content and approve this submission. No conflict of interest exists in this submission.

## CRediT authorship contribution statement

**Rajendran Satheeshkumar:** Conceptualization, Methodology, Writing – original draft. **Kolandaivel Prabha:** Writing – review & editing. **Kailasam Natesan Vennila:** Data curation, Writing – review & editing. **Koray Sayin:** Data curation, Writing – original draft, Writing – review & editing. **Elif Güney:** Data curation. **Werner Kaminsky:** Supervision, Writing – original draft, Writing – review & editing. **Roberto Acevedo:** Writing – review & editing.

## Acknowledgement

Computational part of this work is supported by the Scientific Research Project Fund of Sivas Cumhuriyet University under the project numbers RGD-020.

## Supplementary materials

Supplementary material associated with this article can be found, in the online version, at doi:10.1016/j.molstruc.2022.133552.

## References

[1] A.K. Ghosh, M. Brindisi, Urea derivatives in modern drug discovery and medicinal chemistry, J. Med. Chem. 63 (2019) 2751–2788, doi:10.1021/ACS.JMEDCHEM.9B01541.
[2] A.W. Dombrowski, A.L. Aguirre, A. Shrestha, K.A. Sarris, Y. Wang, The chosen few: parallel library reaction methodologies for drug discovery, J. Org. Chem. (2021), doi:10.1021/ACS.JOC.1C01427/SUPPL_FILE/JO1C01427_SI_001.PDF.
[3] K. Okamoto, M. Ikemori-Kawada, A. Jestel, K. Von König, Y. Funahashi, T. Matsushima, A. Tsuruoka, A. Inoue, J. Matsui, Distinct binding mode of multikinase inhibitor lenvatinib revealed by biochemical characterization, ACS Med. Chem. Lett. 6 (2015) 89–94, doi:10.1021/ML500394M/SUPPL_FILE/ML500394M_SI_001.PDF.
[4] C.C. Ayala-Aguilera, T. Valero, Á. Lorente-Macías, D.J. Baillache, S. Croke, A. Unciti-Broceta, Small molecule kinase inhibitor drugs (1995–2021): medical indication, pharmacology, and synthesis, J. Med. Chem. 65 (2021) 1047–1131, doi:10.1021/ACS.JMEDCHEM.1C00963.
[5] L.A.T. Allen, R.C. Raclea, P. Natho, P.J. Parsons, Recent advances in the synthesis of $\alpha$-amino ketones, Org. Biomol. Chem. 19 (2021) 498–513, doi:10.1039/D0OB02098B.
[6] R.K. Singh, D.N. Prasad, T.R. Bhardwaj, Design, synthesis and evaluation of aminobenzophenone derivatives containing nitrogen mustard moiety as potential central nervous system antitumor agent, Med. Chem. Res. 22 (2013) 5901–5911, doi:10.1007/S00044-013-0582-8/TABLES/6.
[7] J.-P. Liou, C.-W. Chang, J.-S. Song, Y.-N. Yang, C.-F. Yeh, H.-Y. Tseng, Y.-K. Lo, Y.-L. Chang, C.-M. Chang, H.-P. Hsieh, Synthesis and structure–activity relationship of 2-aminobenzophenone derivatives as antimitotic agents, J. Med. Chem. 45 (2002) 2556–2562.
[8] L. Ren, T. Lei, J.X. Ye, L.Z. Gong, Step-economical synthesis of tetrahydroquinolines by asymmetric relay catalytic friedländer condensation/transfer hydrogenation, Angew. Chemie Int. Ed. 51 (2012) 771–774, doi:10.1002/ANIE.201106808.
[9] J. Chen, J. Li, W. Su, Palladium-catalyzed direct addition of 2-aminobenzonitriles to sodium arylsulfinates: synthesis of o-aminobenzophenones, Molecules 19 (2014) 6439–6449, doi:10.3390/MOLECULES19056439.
[10] T. Earmme, E. Ahmed, S.A. Jenekhe, Solution-processed highly efficient blue phosphorescent polymer light-emitting diodes enabled by a new electron transport material, Adv. Mater. 22 (2010) 4744–4748, doi:10.1002/ADMA.201001585.
[11] S.M. Ghelani, Y.T. Naliapara, Design, synthesis, and characterization of 1, 3-disubstituted-1,4-benzodiazepine derivatives, J. Heterocycl. Chem. 53 (2016) 1795–1800, doi:10.1002/JHET.2486.
[12] J. Zhang, C. Yu, S. Wang, C. Wan, Z. Wang, A novel and efficient methodology for the construction of quinazolines based on supported copper oxide nanoparticles, Chem. Commun. 46 (2010) 5244–5246, doi:10.1039/C002454F.
[13] R. Satheeshkumar, K.J. Rajendra Prasad, W. Wen-Long, C. Espinosa-Bustos, C.O. Salas, Solvent-free synthesis of new quinoline derivatives via Eaton's reagent catalysed Friedländer synthesis, ChemistrySelect 7 (2022) e202104416, doi:10.1002/SLCT.202104416.
[14] R. Satheeshkumar, S. Kalaiselvi, K.J. Rajendra Prasad, W.-L. Wang, C.O. Salas, Friedländer's synthesis of quinolines as a pivotal step in the development of bioactive heterocyclic derivatives in the current era of medicinal chemistry, Chem. Biol. Drug Des. (2022), doi:10.1111/CBDD.14044.
[15] R. Satheeshkumar, K. Shanmugaraj, T. Delgado, J. Bertrand, I. Brito, C.O. Salas, Friedländer synthesis of novel polycyclic quinolines using solid sio2/h2so4 catalyst, Org. Prep. Proced. Int. 53 (2021) 138–144, doi:10.1080/00304948.2020.1865069.
[16] F. Xiong, H. Wang, L. Yan, L. Xu, Y. Tao, Y. Wu, F. Chen, Diastereoselective synthesis of pitavastatin calcium via bismuth-catalyzed two-component hemiacetal/oxa-Michael addition reaction, Org. Biomol. Chem. 13 (2015) 9813–9819, doi:10.1039/C5OB01148E.
[17] C.S. Jia, Z. Zhang, S.J. Tu, G.W. Wang, Rapid and efficient synthesis of polysubstituted quinolines assisted by p-toluene sulphonic acid under solvent-free conditions: comparative study of microwave irradiation versus conventional heating, Org. Biomol. Chem. 4 (2006) 104–110, doi:10.1039/b513721g.
[18] C.M. Counceller, C.C. Eichman, B.C. Wray, J.P. Stambuli, A practical, metal-free synthesis of 1H-Indazoles, Org. Lett. 10 (2008) 1021–1023, doi:10.1021/ol800053f.
[19] J. Zhang, D. Zhu, C. Yu, C. Wan, Z. Wang, A simple and efficient approach to the synthesis of 2-phenylquinazolines via sp3 C-H functionalization, Org. Lett. 12 (2010) 2841–2843, doi:10.1021/ol100954x.

[20] B. Cui, S. Jia, E. Tokunaga, N. Shibata, Defluorosilylation of fluoroarenes and fluoroalkanes, Nat. Commun. 9 (2018) 1–8, doi:10.1038/s41467-018-06830-w.
[21] R. Satheeshkumar, R. Shankar, W. Kaminsky, S. Kalaiselvi, V.V. Padma, K.J. Rajendra Prasad, Theoretical and experimental investigations on molecular structure of 7-Chloro-9-phenyl-2,3-dihydroacridin-4(1H)-one with cytotoxic studies, J. Mol. Struct. 1109 (2016) 247–257, doi:10.1016/j.molstruc.2016.01.002.
[22] R. Satheeshkumar, K. Sayin, W. Kaminsky, K.J. Rajendra Prasad, Synthesis, spectral analysis and quantum chemical studies on molecular geometry, chemical reactivity of 7-chloro-9-(2′-chlorophenyl)-2,3-dihydroacridin-4(1H)-one and 7-chloro-9-(2′-fluorophenyl)-2,3-dihydroacridin-4(1H)-one, J. Mol. Struct. 1128 (2017) 279–289, doi:10.1016/j.molstruc.2016.08.080.
[23] A. Mahmood, M. Saqib, M. Ali, M.I. Abdullah, B. Khalid, Theoretical investigation for the designing of novel antioxidants, Can. J. Chem. 91 (2013) 126–130, doi:10.1139/CJC-2012-0356/ASSET/IMAGES/LARGE/CJC-2012-0356F7.JPEG.
[24] R. Satheeshkumar, R. Rajamanikandan, M. Ilanchelian, K. Sayin, K.J.R. Prasad, Synthesis of novel 1,10-phenanthroline derivatives and it used as probes for sensitive detection of Zn2+ and Cd2+ metal ions – Spectroscopic and theoretical approach, Spectrochim. Acta - Part A Mol. Biomol. Spectrosc. 221 (2019) 117196, doi:10.1016/j.saa.2019.117196.
[25] R. Satheeshkumar, K. Sayin, W. Kaminsky, K.J. Rajendra Prasad, Synthesis, spectroscopic, in vitro cytotoxicity and crystal structures of novel fluorinated dispiroheterocycles: DFT approach, Monatshefte Fur Chem. 149 (2018) 141–147, doi:10.1007/s00706-017-2050-5.
[26] R. Jayarajan, R. Satheeshkumar, T. Kottha, S. Subbaramanian, K. Sayin, G. Vasuki, Water mediated synthesis of 6-amino-5-cyano-2-oxo-N-(pyridin-2-yl)-4-(p-tolyl)-2H-[1,2′-bipyridine]-3-carboxamide and 6-amino-5-cyano-4-(4-fluorophenyl)-2-oxo-N-(pyridin-2-yl)-2H-[1,2′-bipyridine]-3-carboxamide – an experimental and computational studies, Spectrochim. Acta - Part A Mol. Biomol. Spectrosc. 229 (2020) 117861, doi:10.1016/j.saa.2019.117861.
[27] R. Satheeshkumar, K. Sayin, W. Kaminsky, K.J. Rajendra Prasad, Indium triflate and ionic liquid-mediated Friedländer synthesis of 2-acylquinolines, Synth. Commun. 47 (2017) 1940–1954, doi:10.1080/00397911.2017.1357185.
[28] R. Satheeshkumar, R. Montecinos, A. Vera, K.J. Rajendra Prasad, W. Kaminsky, C.O. Salas, Experimental and theoretical physicochemical study of a new dispirocompound: 4′-(4-fluorophenyl)-2′,7-dimethyl-1,4-dihydro-3H-dispiro[cyclopent[b]indol-2,5′-[1,2]oxazinan-6′,3′-indolin]-2′,3–dione, J. Mol. Struct. 1227 (2021) 129431, doi:10.1016/j.molstruc.2020.129431.
[29] R. Satheeshkumar, R. Shankar, W. Kaminsky, K.J. Rajendra Prasad, Novel synthetic and mechanistic approach of TFA catalysed friedländer synthesis of 2-acylquinolines from symmetrical and unsymmetrical 1,2-diketones with o-aminoarylketones, ChemistrySelect 1 (2016) 6823–6829, doi:10.1002/slct.201601624.
[30] A. Mahmood, Photovoltaic and charge transport behavior of diketopyrrolopyrrole based compounds with A–D–A–D–A skeleton, J. Clust. Sci. 30 (2019) 1123–1130, doi:10.1007/S10876-019-01573-0/TABLES/4.
[31] A. Mahmood, M.I. Abdullah, S.U.D. Khan, Enhancement of nonlinear optical (NLO) properties of indigo through modification of auxiliary donor, donor and acceptor, Spectrochim. Acta Part A Mol. Biomol. Spectrosc. 139 (2015) 425–430, doi:10.1016/J.SAA.2014.12.038.
[32] Z. Kökbudak, S. Akkoç, H. Karataş, B. Tüzün, G. Aslan, In silico and in vitro antiproliferative activity assessment of new Schiff bases, ChemistrySelect. 7 (2022) e202103679, doi:10.1002/SLCT.202103679.
[33] S. Akkoç, B. Tüzün, A. Özalp, Z. Kökbudak, Investigation of structural, electronical and in vitro cytotoxic activity properties of some heterocyclic compounds, J. Mol. Struct. 1246 (2021) 131127, doi:10.1016/J.MOLSTRUC.2021.131127.
[34] M. Gömeç, F. Yulak, H. Gezegen, M. Özkaraca, K. Sayin, H. Ataseven, Synthesis of diaryl urea derivatives and evaluation of their antiproliferative activities in colon adenocarcinoma, J. Mol. Struct. 1254 (2022) 132318, doi:10.1016/J.MOLSTRUC.2021.132318.
[35] A. Aktas, B. Tuzun, A.H. Taskin Kafa, K. Sayin, H. Ataseven, How do arbidol and its analogs inhibit the SARS-CoV-2? Bratislava Med. J. 121 (2020) 705–711, doi:10.4149/BLL_2020_115.
[36] M.A. Gedikli, B. Tuzun, A. Aktas, K. Sayin, H. Ataseven, Are clarithromycin, azithromycin and their analogues effective in the treatment of COVID19? Bratislava Med. J. 122 (2021) 101–110, doi:10.4149/BLL_2021_015.
[37] K. Okamoto, M. Ikemori-Kawada, A. Jestel, K. von Konig, Y. Funahashi, T. Matsushima, A. Tsuruoka, A. Inoue, J. Matsui, Distinct binding mode of multikinase inhibitor lenvatinib revealed by biochemical characterization, ACS Med. Chem. Lett. 6 (2015) 89–94.
[38] R. Dennington, T.A. Keith, J.M. Millam, GaussView, Version 6.1, Semichem Inc., Shawnee Mission. KS,. (2016).
[39] M.J. Frisch, G.W. Trucks, H.B. Schlegel, G.E. Scuseria, M.A. Robb, J.R. Cheeseman, G. Scalmani, V. Barone, G.A. Petersson, H. Nakatsuji, X. Li, M. Caricato, A.V. Marenich, J. Bloino, B.G. Janesko, R. Gomperts, B. Mennucci, H.P. Hratchian, J.V. Ortiz, A.F. Izmaylov, J.L. Sonnenberg, D. Williams-Young, F. Ding, F. Lipparini, F. Egidi, J. Goings, B. Peng, A. Petrone, T. Henderson, D. Ranasinghe, V.G. Zakrzewski, J. Gao, N. Rega, G. Zheng, W. Liang, M. Hada, M. Ehara, K. Toyota, R. Fukuda, J. Hasegawa, M. Ishida, T. Nakajima, Y. Honda, O. Kitao, H. Nakai, T. Vreven, K. Throssell, J.J.A. Montgomery, J.E. Peralta, F. Ogliaro, M.J. Bearpark, J.J. Heyd, E.N. Brothers, K.N. Kudin, V.N. Staroverov, T.A. Keith, R. Kobayashi, J. Normand, K. Raghavachari, A.P. Rendell, J.C. Burant, S.S. Iyengar, J. Tomasi, M. Cossi, J.M. Millam, M. Klene, C. Adamo, R. Cammi, J.W. Ochterski, R.L. Martin, K. Morokuma, O. Farkas, J.B. Foresman, D.J. Fox, Gaussian 16, Revision C.01, Gaussian, Inc., Wallingford CT,. (2016).
[40] R.A. Friesner, R.B. Murphy, M.P. Repasky, L.L. Frye, J.R. Greenwood, T.A. Halgren, P.C. Sanschagrin, D.T. Mainz, Extra precision glide: docking and scoring incorporating a model of hydrophobic enclosure for protein-ligand complexes, J. Med. Chem. 49 (2006) 6177–6196, doi:10.1021/jm051256o.
[41] Schrödinger Release 2021-4: LigPrep, Schrödinger, LLC, New York, NY, (2021).
[42] Schrödinger Release 2021-4: FEP+, Schrödinger, LLC, New York, NY, (2021).
[43] Schrödinger Release 2021-4: Protein Preparation Wizard; Epik, Impact, Schrödinger, LLC, New York, NY; Prime, Schrödinger, LLC, New York, NY, (2021).
[44] M. Gerber, S. Goel, R. Maitra, In silico comparative analysis of KRAS mutations at codons 12 and 13: structural modifications of P-Loop, switch I&II regions preventing GTP hydrolysis, Comput. Biol. Med. 141 (2022) 105110, doi:10.1016/J.COMPBIOMED.2021.105110.
[45] Z. Otwinowsky, W. Minor, Processing of X-ray diffraction data collected in oscillation mode, in: C.W. Carter, R.M. Sweet (Eds.), Methods Enzymol, Elsevier, 1997, pp. 307–326.
[46] G.M. Sheldrick, SHELXT – integrated space-group and crystal-structure determination, Acta Crystallogr. Sect. A Found. Adv. 71 (2015) 3–8, doi:10.1107/S2053273314026370.
[47] A. Altomare, M.C. Burla, M. Camalli, G.L. Cascarano, C. Giacovazzo, A. Guagliardi, A.G.G. Moliterni, G. Polidori, R. Spagna, SIR97: a new tool for crystal structure determination and refinement, J. Appl. Crystallogr. 32 (1999) 115–119, doi:10.1107/S0021889898007717.
[48] A. Altomare, G. Cascarano, C. Giacovazzo, A. Guagliardi, Completion and refinement of crystal structures with SIR92, J. Appl. Crystallogr. 26 (1993) 343–350, doi:10.1107/S0021889892010331.
[49] G.M. Sheldrick, SHELXL-97, program for the refinement of crystal structures, Univ. Göttingen, Ger. (1997) https://ci.nii.ac.jp/naid/10011246258/.
[50] G.M. Sheldrick, Crystal structure refinement with SHELXL, Acta Crystallogr. Sect. C Struct. Chem. 71 (2015) 3–8, doi:10.1107/S2053229614024218.
[51] D. Waasmaier, A. Kirfel, New analytical scattering-factor functions for free atoms and ions, Acta Crystallogr. Sect. A Found. Adv. 51 (1995) 416–431, doi:10.1107/S0108767394013292.
[52] L.J. Farrugia, ORTEP-3 for Windows - a version of ORTEP-III with a graphical user interface (GUI), J. Appl. Crystallogr. 30 (1997) 565–565, doi:10.1107/S0021889897003117.
[53] L.H. Al-Wahaibi, J. Joubert, O. Blacque, N.H. Al-Shaalan, A.A. El-Emam, Crystal structure, Hirshfeld surface analysis and DFT studies of 5-(adamantan-1-yl)-3-[(4-chlorobenzyl)sulfanyl]-4-methyl-4H-1,2,4-triazole, a potential 11$\beta$-HSD1 inhibitor, Sci. Rep. 9 (2019) 1–11, doi:10.1038/s41598-019-56331-z.